Fabrication and properties of zirconia/hydroxyapatite composite scaffold based on digital light processing

Article (Accepted Version)

Fabrication and properties of zirconia/hydroxyapatite composite scaffold based on digital light processing

Ying Cao[a,1], Tianshu Shi[b,1], Chen Jiao[a], Huixin Liang[a], Ruoyu Chen[c], Zongjun Tian[a,d,*], Anchao Zou[a] Youwen Yang[e], Zhen Wei[f], Changjiang Wang[g], Lida Shen[a,**]

[a] College of Mechanical and Electrical Engineering, Nanjintg University of Aeronautics and Astronautics, Nanjing, 210016, China

[b] Department of Sports Medicine and Adult Reconstructive Surgery, Drum Tower Hospital, School of Medicine, Nanjing University, 321 Zhongshan Road, Nanjing, 210008, China

[c] College of Materials Science and Technology, Nanjing University of Aeronautics and Astronautics, Nanjing, 211106, China

[d] NUAA Institute of Additive Manufacturing (3D Printing), Nanjing, 210016, China

[e] Jiangxi University of Science and Technology, Ganzhou, 341000, China

[f] Jiangsu pharmaceutical association, Zhong Shan East Road, 210016, Nanjing, China

[g] Department of Engineering and Design, University of Sussex, Sussex House, Brighton, BN19RH, United Kingdom

∗ Corresponding author.

∗∗ Corresponding author. College of Mechanical and Electrical Engineering, Nanjing University of Aeronautics and Astronautics, Nanjing, 210016, China.

E-mail addresses: tianzj@nuaa.edu.cn (Z. Tian), ldshen@nuaa.edu.cn (L. Shen).

[1] These authors contributed equally.

Abstract

Zirconia and hydroxyapatite(HA) are two typical implant materials, which have the advantages of excellent mechanical strength and good biological activity respectively. It was found that composite material had good biocompatibility and mechanical strength compared to the single material.

In this paper, the porous scaffolds of ZrO_2/HA composite were formed by digital light processing (DLP) technology and their performance were evaluated. Cell experiments showed that the addition of HA had a positive effect on cell proliferation and differentiation. Mechanical tests showed that the composite scaffold with 10 wt.% HA had the best compressive capacity due to the pinning and bridging effect of a small amount of HA grains. When scaffolds were immersed in the simulated body fluid (SBF), the compressive strengths of the composite scaffolds decreased within the first 14 days and gradually increased after 14 days. The reason for this phenomenon was the degradation of calcium phosphate components and the deposition of apatite. By the 28th day, the compressive strengths of all the composite scaffolds increased to over 20MPa, close to that of the zirconia scaffolds during the same period (25MPa). The compressive strengths of all scaffolds met the requirement of cancellous bone during the entire soaking period, and the composite scaffolds have potential application value in bone repair.

Keywords: nanocomposites; bone scaffolds; digital light processing; vitro properties

1. Introduction

Bones have a strong ability to self-repair some minor damage. However, for bone defects exceeding the critical size, artificial assistance is necessary to complete bone reconstruction, transplantation and

replacement [1]. Autologous and allogeneic bone grafts have a better adaptability for bone grafting, but they cannot be widely applied because of their limited quantity, ambiguous sources and disturbing security [2]. As they are unable to meet the needs of a growing number of patients with bone defects, researchers have turned their attention to artificial bone repair materials. At present, the common artificial bone repair materials are metal [3, 4], ceramic [5, 6], high polymer [7], and composite materials [8, 9].

Generally, artificial bone repair materials must have good compatibility with surrounding cell tissue to promote the repair and healing of the defect site. In addition, implants must also partly meet the functional requirements of the defects, such as support, movement, and protection. These functions put high demands on the biological and mechanical properties of implants. Calcium phosphate and calcium silicate ceramic are commonly used as bone repair materials because they have similar composition and structure as bones. Among them, hydroxyapatite (HA), the main inorganic component of biological hard tissue, has been proven to have good bioactivity and osteoconductivity [10, 11]. However, its mechanical properties are poor, for example, its modulus of elasticity is too large and the fracture toughness is too small compared to human bone [12]. Degradable ceramic materials such as tricalcium phosphate (TCP), biphasic calcium phosphate (BCP), and calcium silicate have been proven to have good osteogenic ability, and can be completely degraded in vivo environments and eventually replaced by new bones. This can avoid the hidden trouble caused by foreign bodies [13]. Even so, the degradation rate of this kind of ceramic in the body is often too fast, and does not match the osteogenesis speed. In addition, its mechanical properties are poor, and will be further weakened during the degradation process and cannot meet the requirements over a long period of time [14]. All these properties limit the use of degradable ceramics as load-bearing bone repair materials; they are usually used as hard tissue fillers. As a bio-inert

ceramic material, zirconia has high mechanical properties, good wear resistance, and can be stable in vivo for a long time [15].

Nowadays, researchers have introduced other materials to build composite degradable materials which can make up for the deficiencies of a single material and promise to have a wider range of application in bone tissue repair. Brzezinska-Miecznik et al. [16] combined HA with zirconia and sintered the composite. It was found that zirconia caused the decomposition of HA, resulting in the formation of β-TCP and CaO-ZrO2 solid solution. Kong et al. [17] found that the addition of alumina could reduce the reaction between zirconia and HA. A composite doped with 40% HA could attain biological activity comparable to that of pure HA and had better mechanical properties. Kumar et al. [18] incorporated nano-zirconia powder of different mass fractions (0-25 wt.%) into nano-HA powder and pressed it into shape. They found that the composites containing 20 wt.% ZrO_2 performed better than pure HA and other ratios of composites.

In addition to compounding multiple materials, it is also possible to further regulate the mechanical properties by introducing porous structures to meet the requirements of human implants (Young's modulus of the cortical bone is between 15 and 20 GPa and that of cancellous bone is between 0.1 and 2 GPa. Compressive strength of the cortical bone is 100 to 200 MPa while that of cancellous bone is 2 to 20 MPa)[19]. Moreover, the pore structures with suitable sizes can transport nutrients and metabolites, and provide space for cell tissue growth [20].

Considering the fabrication, additive manufacturing can customize the structure and function by design 3D models of implants for which the appearance, porosity, internal pore shape, and other parameters can be controlled. Lohfeld et al. [21] printed polycaprolactone(PCL) and PCL/TCP into bone

tissue engineering scaffolds using SLS process, and the mechanical properties were altered by adjusting the material ratio and porosity. Wang et al. [22] used a continuous filament writing method with a sol-gel ink. The structure and pore size could be well controlled, and the feature size of the filaments could be tens of microns or even finer. Liu et al. [23] used a self-developed DLP printer to print HA ceramic samples with good and biocompatibility. Furthermore, researchers have also explored the factors of DLP ceramic forming, optimized the material formulation and printing parameters, and ultimately obtained high-precision, complex ceramic components [24-26].

In this paper, ZrO_2 was combined with HA to produce a partially degraded, porous scaffold which can improve the biological activity of the material. In addition, it can retain good mechanical properties during the healing phase of bone injury and reduce the impact on the function of the injured part. To evaluate the biological properties of ZrO_2/HA scaffolds, simulated body fluid (SBF) soaking tests and in vitro cell tests were carried out to determine the biological activity, osteogenesis, and mineralization of the porous bone scaffolds The changes of the compressive strength of the scaffolds under the SBF condition were also evaluated in detail.

2. Materials and methods

2.1 Fabrication of ZrO_2/HA scaffolds

To fabricate ZrO_2/HA porous bone scaffolds, nano zirconia powder (containing 5% Y_2O_3, particle size: 300 nm, Saint-Gobain, China) and HA powder (particle size: 60 nm, Xian Fenghe Biotech Co., Ltd., China) were used as raw materials. 0 wt.%, 10 wt.%, 20 wt.% and 30 wt.% HA powder were respectively added into ZrO_2 to obtain different proportions of composite powder. Two kinds of material powders were

mixed evenly with a ball mill for 4 h. The homogeneous ceramic slurry was obtained by stirring the composite powder with added photosensitive resin (Shanghai Guangyi Chemical Co., Ltd., China) and dispersant (sodium polyacrylate, Hebei Jinhong Chemical Co., Ltd., China) for 1 h.

The porous three-dimensional bone scaffold model was designed according to the previous research in our team [23], and the porosity was 54.6%. The model data were imported into a DLP light-curing printer developed by Nanjing University of Aeronautics and Astronautics. The thickness of each printing layer used for printing composite ceramic slurry. was 0.02 mm. After printing, the green body of the scaffold was washed in absolute ethanol for 5 min via ultrasound to remove the extra slurry on the surface, and the extra slurry in the hole was eventually removed via air gun. After the green body was dried, it was put in a tube furnace for heat treatment at 500 °C for 4 h. The organic materials in the body, such as resin, were removed. Finally, the green body was sintered at 1400 °C for 1.5 h to obtain a composite porous scaffold. The specific heating curve is shown in Fig. 1. According to this method, two kinds of models were designed, one with a side length of 7.5 mm and height of 15 mm, the other with a side length of 10 mm and height of 5 mm. The scaffolds were then fabricated for compression tests and cell tests. The fabrication and testing process of the scaffolds are shown in Fig. 2.

2.2 Scaffold characteristics

The optical images of the unsintered and sintered bodies were obtained by a camera, and their dimensions were measured to calculate the shrinkage ratios of the sintered bodies. A scanning electron microscope (SEM, S4800, Hitachi Instruments, Japan) equipped with an energy-dispersive X-ray spectroscope (EDS) was used to observe the surface morphologies and element distributions of the scaffolds. The phase composition was identified and analyzed via X-ray diffractometry (XRD, Ultima IV,

40kV/30mA, Rigaku, Japan) with a Cu-Kα radiation over a 2θ range from 20° to 70° with a scan speed of 4° min^{-1} and a step size of 0.02°.

2.3 Cell tests

2.3.1 Cell culture

The mouse osteoblast precursor cell line (MC3T3-E1) was cultured with scaffolds to evaluate the effects of different HA contents on cell adhesion, proliferation and differentiation. MC3T3-E1 cells were cultured in Minimum Essential Medium Alpha (α-MEM containing 10% fetal bovine serum and 4% penicillin-streptomycin, Gibco, USA) at 37 °C under a 5% CO_2 atmosphere. The culture medium was changed every 2-3 days and the cells were passed every 4-5 days to ensure normal growth.

2.3.2 Cell adhesion

The scaffolds were ultrasonically cleaned and autoclaved, and then were placed in a 24-well plate and inoculated with 1 mL of cell suspension (10^5 cells/mL) in every well. After culturing for 1 day, the cells adhered on the surface of the scaffolds were observed via SEM. Briefly, the scaffolds were washed with phosphate buffered saline (PBS) twice, and fixed in 3% glutaraldehyde at 4 °C overnight. Then, they were dehydrated in ethanol solution with different concentrations (30%, 50%, 70%, 85%, 90%, 100%, 100%). Finally, the samples were vacuum freeze-dried before gold sputtering for SEM observation. After culturing for 4 days, the cell-seeded scaffolds were fixed in 4% paraformaldehyde for 10 minutes. They were then stained with phalloidin (AAT Bioquest, USA) for 30 minutes and then with DAPI (4',6-diamidino-2-phenylindole, AAT Bioquest, USA) for another 10 minutes. The cell adhesion inside the scaffolds was observed under a confocal laser scanning microscope (CLSM, FV3000, Olympus,

Japan).

2.3.3 Cell proliferation and differentiation

A Cell Counting Kit-8 (CCK-8, Bimake, USA) was used to evaluate the effect of scaffolds with different HA contents on cell viability. The samples in the 24-well plate (originally 10^4 cells/well) were cultured for 1, 4 and 7 days. Then, the cell medium in each well was refreshed with 1 mL of new medium containing 10% CCK-8 solution After incubating at 37 °C for 2 h, 100 μL of liquid was transferred into a new 96-well plate, and the optical density (OD) value of each well was measured at a wavelength of 450 nm by a microplate reader (SpectraMax M3, Molecular Devices, USA).

To evaluate the effect of composite scaffolds on cell mineralization, the autoclaved scaffolds were placed in a 12-well plate, and 2 mL of MC3T3-E1 cells at a concentration of 10^4 cells/ml were inoculated and cultured for 14 days. After culturing, cells were washed by PBS, fixed in 4% paraformaldehyde for 10 minutes and then incubating with 0.1% Alizarin Red S (ARS, pH = 8.3, Macklin, China) at 37 °C for 30 minutes. The calcium deposition produced by cell mineralization could be detected by red staining.

2.4 SBF tests

2.4.1 Degradation and bioactivity

The degradation performance and biological activity of the composite scaffolds were evaluated by soaking the samples in SBF (simplified body fluid, pH = 7.4, Leagene, China). Each scaffold was soaked in 50 mL of SBF and placed in a 37 °C incubator with 5% CO_2. They were taken out at different time periods (1, 4, 7, 14 days). After the samples were cleaned and dried, the weight changes were recorded.

The surface morphologies were observed by SEM, and the composition of the surface materials were analyzed.

2.4.2 Compressive Strength

A universal testing machine (AG-Xplus, crosshead speed = 0.1 mm/s, Shimadzu, Japan) with a load of 10kN was used to measure the compressive strength of the scaffolds soaked for different time periods (1, 4, 7, 14, 21, 28 days) in SBF. Before they were tested, the scaffolds were first dried at 60 °C for 8 h. The untreated scaffolds were also tested in a dry state.

3. Results and discussion

3.1 Surface morphology and composition analysis

Fig. 3(a) presents the whole shapes of the scaffolds before and after sintering. Scaffolds with different HA additions (0 wt.%, 10 wt.%, 20 wt. %, 30 wt.%, hereinafter referred to as ZH0, ZH10, ZH20 and ZH30, respectively) have similar macrostructures. The unsintered body had a significant shrinkage after high-temperature heat treatment. Table 1 shows the average sizes of the model, the unsintered body and the sintered body. The shrinkage rate in the length direction was calculated to be about 23.27%. The shrinkage in the height direction was about 28.33%, which was slightly higher than that in the length direction. This may be related to the DLP forming process. The green body must be separated from the slurry tank after each layer is printed; the process will produce a large pulling force on the part that has been printed, and the bonding tightness between the layers will be slightly lower than that in other places. As a result, the intergranular voids between the layers after debinding are larger, but the voids could be

eliminated and the particles could be tightly bound after high-temperature sintering. Therefore, greater shrinkage appears in the height direction. In addition, studies have shown that gravity can promote shrinkage in the height direction to a certain extent [27]. Fig. 3(b-e) present the surface morphologies of different scaffolds. The grains of the ZH0 scaffolds can be clearly observed and have sizes of about 200-500 nm. With the addition of HA, clear differences in brightness and size between the grains were found via SEM. Specifically, the dark grains of different sizes pointed by arrows in Fig. 3(c-e) were embedded in the small zirconia grains. The number and size of the dark grains both increased as the amount of HA added increased. The large grains in the ZH30 group gradually became one piece, which can be seen in Fig. 3(e). These phenomena may be related to the reaction of HA and zirconia at high temperatures [28].

To determine these altered grains, we analyzed the compositions of the scaffolds, and the XRD results were shown in Fig. 4. After high-temperature sintering at 1400 °C, tricalcium phosphate (TCP) appeared in the samples, and should be the decomposition product of HA at this temperature [29]. On the one hand, TCP is a bioactive calcium phosphate ceramic with a higher degradation rate than HA. On the other hand, biphasic calcium phosphate (BCP) consisting of TCP and undecomposed HA has been proven to have better mechanical properties and osteogenetic ability than the single phase [14, 30]. In addition, calcium oxide, another decomposition product of HA, can dissolve into the interior of the zirconia crystal, changing the original crystal structure [31]. This can be confirmed by apparent cubic zirconia diffraction peaks in the composite scaffold. As is shown in **Error! Reference source not found.**(b), the EDS mapping of the ZH20 scaffolds indicates that the calcium was homogeneously distributed on the surface of the sample. Moreover, the EDS analysis of local grains, which is presented in **Error! Reference**

source not found.(c), revealed that the content of calcium in the dark grains was significantly higher than that in light grains. Many studies discovered the dark particles, which were considered to be hydroxyapatite or other calcium phosphates [17, 32-34].Therefore, dark grains should contain more calcium phosphate components.

In short, all the scaffolds had a significant shrinkage after sintering, and component changes occurred in the HA-added scaffolds. TCP appeared in the samples with the decomposition of HA, which caused the dark grains of calcium phosphate embedded in the small zirconia grains. Moreover, the number and size of the dark grains both increased as the HA increased.

3.2 Cytocompatibility

To evaluate the biological properties of the composite scaffolds, MC3T3-E1 cells were inoculated on each scaffold. Fig. 6(a) depicts the cells adhered on the surfaces of scaffolds after culturing for 1 day . After 4 days, cells grown into the scaffolds were observed. Fig. 6(b) shows the fluorescence staining of the cells inside the scaffolds. According to the figures, all scaffolds had cell attachment after incubating for 1 day, and each group of cells grew well. In addition, there were a large number of cells growing inside the scaffolds after culturing for 4 days. Specifically, more cells were attached inside the scaffold with HA added, and the cells gradually became confluent (see the ZH30 group in Fig. 6(b)), which demonstrates that ZrO_2/HA composite scaffolds have good biocompatibility.

To further verify the effect of HA content on cell viability, the CCK-8 method was used to evaluate the viability of MC3T3-E1 cells on different ceramic scaffolds for 1, 4, 7 days. The results are presented in Fig. 7. The OD values of each group achieved a steady increase over time, which indicates that the HA-added scaffolds had no obvious adverse effect on cell viability. The OD values of ZH20 and ZH30 on

the 4th and 7th day were significantly higher than those of the ZH0 group ($p < 0.05$). These results demonstrated that the composite scaffold with 20 wt.% and 30 wt.% HA had a positive effect on MC3T3-E1 cell proliferation.

Previous research showed that calcium phosphate-based ceramics have good biocompatibility and osteoinductivity [35-37]. Calcium, phosphate ions and other components, considered to play an active role in the osteogenesis process, can be dissolved from the ceramics in vivo environments. To evaluate the effect of composite scaffolds on MC3T3-E1 cell mineralization, the cells were cultured for 14 days with the scaffolds, and the ARS staining results showed that almost no calcium deposition occurred in the control group without scaffolds or in the ZH0 group (see Fig. 8(a) and 8(b)). With the addition of HA, clear calcium deposition began to appear. There are only a few red depositions with a small number and area in ZH10, which can be observed in Fig. 8(c). When 20wt.%HA was added to the composite scaffold, large calcium nodules began to form, as shown in Fig. 8(d). Fig. 8(e) indicates that more calcium depositions became darker red with a wider scope in the ZH30 group. This phenomenon demonstrated that HA-added scaffolds promotes the mineralization of osteoblasts, which has positive significance for the repair of bone defects. Previous research showed that calcium phosphate-based ceramics could promote bone formation because their composition was similar to bone [38]. Moreover, Bao et al. [39] believed that such ceramics could recognize and interact with the components in body fluids, and biomolecules relevant to osteogenesis could be adsorbed onto the surface of the ceramics, forming a local microenvironment, which was considered beneficial for osteogenesis and differentiation. In addition, the porous structures with suitable size of scaffolds can provide the climbing conditions and growing space required for osteoblasts [40] .

In summary, compared with the ZrO_2 scaffold, composite scaffolds had better biocompatibility, and 20 wt.% or 30 wt.% HA-added scaffolds could significantly promote the proliferation and differentiation of MC3T3-E1 cells, which could be important for bone repair.

3.3 Apatite deposition and degradation in SBF

The surface morphology of each scaffold changed after soaking in SBF (see Fig. 9). After 7 days of soaking, sporadic white apatite was deposited onto the surface of the HA-added scaffolds. After 14 days, the surface of each scaffold had a certain scale of white apatite deposition. The apatite on the surface of ZH0 was mostly distributed in the form of small-area fragments, while that on the HA-added scaffolds continuously grew like snowflakes. In addition to the apatite deposition, some degradation occurred to the scaffolds. After soaking for 4 days, ZH10, ZH20 and ZH30 groups had obvious pores. Fig. 10 reveals the occurrence of degradation behavior. Nano-scale micropores appeared on the surfaces of large calcium phosphate grains and near grain boundaries. As the soaking time increased, the number and range of micropores gradually increased, eventually leading to the shedding of entire particles or the parts connected by micropores. This study showed a similar pattern of results compared to previous studies[14, 41].

The mass loss of each scaffold after soaking in SBF is shown in Fig. 11. With the increase of the soaking time, the ZH0 group exhibited almost no mass loss, and the mass increased slightly after 14 days, which was consistent with the deposition of apatite on the ZH0 scaffold during this period (see Fig. 9(a3)). The other three scaffolds all had mass loss after soaking, and the loss weight increased with the increase of HA content and soaking time. Moreover, the mass loss rate of scaffolds increased rapidly in the first 7 days and then slowed down gradually. Combined with the surface morphology analysis of the scaffolds

during this time period, there was not much apatite deposition on the surface after the first 7 days. At that time, the degradation rate of calcium phosphate was greater than the generation rate of apatite, resulting in a large mass loss rate. After soaking for 14 days, a large amount of apatite had appeared on the surface of the scaffolds, which could compensate for the loss of partial mass degradation, so the rate of mass loss was reduced after 7 days.

Above all, the composite scaffolds were degraded when soaking in SBF, and had more mass loss with the increase of HA content and soaking time. However, partial mass loss could be compensated by apatite deposition which occurred after 7 days.

3.4 Compressive strength in SBF

Fig. 12(a) shows the compressive strength and compressive modulus curves calculated from the cross-sectional areas of the scaffolds. As HA increased, the compressive capacity of the scaffolds first increased and then decreased. All scaffolds met the requirements for cancellous bone strength (compressive strength varied between 2 and 20 MPa, and Young's modulus was between 0.1 and 2 GPa) [19]. Interestingly, when 10 wt.% HA was added, the composite scaffold exhibited a higher compressive strength of 52.25 MPa while that of the ZH0 scaffold was 39.99 MPa, which is different from some previous research [42, 43]. The possible reason for this is the "pinning" effect of the nano-hydroxyapatite on the matrix, and Fig. 12(b) shows that a crack produced by a transgranular fracture in the zirconia matrix had deflected when meeting large particles considered to be calcium phosphate, and Fig. 12(c) shows that the calcium phosphate particle bridged at the crack, creating a reverse closure effect on both sides of the matrix. This can increase the strength of the material. In addition, there are differences in the thermal expansion coefficients of zirconia and HA. A small amount of HA evenly dispersed in the

zirconia matrix could result in a residual stress field after sintering, and the strength of the composite could thereby be improved [44, 45]. However, as HA increased, the reaction between HA and zirconia increased as well, which weakened the overall strength of the material [46].

The compression performance of the scaffolds immersed in SBF for different times was tested, and the results are provided in Fig. 13(a). After soaking, the compressive strength of each scaffold changed in different degrees. After 1-day soaking, the compressive strength exhibited a large decrease. The reason why the compressive strength of the ZH0 was degraded may be that the uncompacted grains fell off during the soaking process. However, after 4 days, the decline was small and gradually stabilized. After 28 days, 63.5% strength was retained in ZH0. The strength of the HA-doped scaffolds decreased in the first 14 days with the increase of soaking time, and the compressive strengths of ZH10, ZH20 and ZH30 at 14 days decreased to 15.8MPa, 8.5 MPa and 3.6 MPa, respectively. Compared with the scaffolds before soaking, the decline rates were 69.8%, 65.9% and 72.5% respectively, but the composite scaffolds still reached the requirements for cancellous bone strength. After 14 days, the compressive strength of each scaffold showed an obvious increase. On the 28th day, the compressive strengths of the three HA-added groups were close to that of ZH0 (25.41 MPa), and were all above 20 MPa. Moreover, for ZH30, the compressive strength of the scaffolds soaked for 28 days was even higher than that of the unsoaked ones. The gaps formed by degradation during the soaking process are shown in Fig. 13(b), and they were filled with the apatite deposition as shown in Fig. 13(c), which made up for the partial loss of strength.

In general, the composite scaffolds with 10 wt.% HA had better compressive capacity due to the pinning and bridging effect of HA grains. Under the combined action of the degradation of calcium phosphate and the deposition of apatite, the compressive strengths of the composite scaffolds soaking in

SBF first decreased and then gradually increased, but all reached the requirements for cancellous bone strength during the entire soaking period.

4. Conclusion

A partially degraded ZrO_2/HA scaffold can be obtained by the DLP method, and the HA in the composite scaffolds transformed into BCP after sintering. Compared with the ZrO_2 scaffold, compo site scaffolds with 20 wt.% or 30 wt.% HA had better biological activity and can promote proliferation and differentiation of MC3T3-E1 cells, which had potential implications for bone repair.

The scaffolds can achieve a certain range of controllable mechanical properties by adjusting the ratio of the two ceramic materials. When HA 10 wt.% was added, the compressive strength of scaffold was improved to 52.25MPa while that of ZrO_2 scaffold was 39.99MPa. However, when the proportion of HA increased to 20 wt.%, the compressive strength began to decrease.

When the scaffolds were soaking in SBF, the compressive strengths of the composite scaffolds first decreased and then increased under the combined effects of calcium phosphate degradation and apatite deposition. Compared with the composite scaffolds before soaking, the decline rates of compressive strengths were all around 70% after 14 days. However, by the 28th day, the compressive strengths of the composite scaffolds increased to over 20MPa, which were close to that of the zirconia scaffolds at the same period (25MPa). All the scaffolds reached cancellous bone strength requirement during the entire soaking period.

Acknowledgements

This work is supported by National Natural Science Foundation of China (Grant No. U1537105 and No. U1532106), National Key Research and Development Program (Grant No. 2018YFB1105400) and Jiangsu Province Key Research and Development Program (Grant No. BE2016010-3). The authors also extend their sincere thanks to those who contributed in instructions and experiments work.

Reference

[1] D.W. Jang, R.A. Franco, S.K. Sarkar, B.T. Lee, Fabrication of porous hydroxyapatite scaffolds as artificial bone preform and its biocompatibility evaluation, ASAIO J, 60 (2014) 216-223. https://doi.org/10.1097/MAT.0000000000000032.

[2] M.A. Asselmeier, R.B. Caspari, S. Bottenfield, A review of allograft processing and sterilization techniques and their role in transmission of the human immunodeficiency virus, The American Journal of Sports Medicine, 21 (1993) 170-175. https://doi.org/10.1177/036354659302100202.

[3] X. Shen, Y. Zhang, P. Ma, L. Sutrisno, Z. Luo, Y. Hu, Y. Yu, B. Tao, C. Li, K. Cai, Fabrication of magnesium/zinc-metal organic framework on titanium implants to inhibit bacterial infection and promote bone regeneration, Biomaterials, 212 (2019) 1-16. https://doi.org/10.1016/j.biomaterials.2019.05.008.

[4] Y. Yang, F. Yuan, C. Gao, P. Feng, L. Xue, S. He, C. Shuai, A combined strategy to enhance the properties of Zn by laser rapid solidification and laser alloying, J Mech Behav Biomed Mater, 82 (2018) 51-60. https://doi.org/10.1016/j.jmbbm.2018.03.018.

[5] C. Gao, P. Feng, S. Peng, C. Shuai, Carbon nanotube, graphene and boron nitride nanotube reinforced bioactive ceramics for bone repair, Acta Biomater, 61 (2017) 1-20. https://doi.org/10.1016/j.actbio.2017.05.020.

[6] L. Li, H. Hu, Y. Zhu, M. Zhu, Z. Liu, 3D-printed ternary SiO2CaO P2O5 bioglass-ceramic scaffolds with tunable compositions and properties for bone regeneration, Ceramics International, 45 (2019) 10997-11005. https://doi.org/10.1016/j.ceramint.2019.02.183.

[7] Q. Zhang, B. Shi, J. Ding, L. Yan, J.P. Thawani, C. Fu, X. Chen, Polymer scaffolds facilitate spinal cord injury repair, Acta Biomaterialia, 88 (2019) 57-77. https://doi.org/10.1016/j.actbio.2019.01.056.

[8] B. Chen, K.Y. Yin, T.F. Lu, B.Y. Sun, Q. Dong, J.X. Zheng, C. Lu, Z.C. Li, AZ91 Magnesium Alloy/Porous Hydroxyapatite Composite for Potential Application in Bone Repair, Journal of Materials Science & Technology, 32 (2016) 858-864. https://doi.org/10.1016/j.jmst.2016.06.010.

[9] Y.W. Yang, X.N. Guo, C.X. He, C.D. Gao, C.J. Shuai, Regulating Degradation Behavior by Incorporating Mesoporous Silica for Mg Bone Implants, Acs Biomaterials Science & Engineering, 4 (2018) 1046-1054. https://doi.org/10.1021/acsbiomaterials.8b00020.

[10] d.B.J. D, v.B.C. A, D.J. E, Initial bone matrix formation at the hydroxyapatite interface in vivo,

Journal of Biomedical Materials Research Part A, 29 (2010). https://doi.org/10.1002/jbm.820290113
[11] S.C. Cox, J.A. Thornby, G.J. Gibbons, M.A. Williams, K.K. Mallick, 3D printing of porous hydroxyapatite scaffolds intended for use in bone tissue engineering applications, Mater Sci Eng C Mater Biol Appl, 47 (2015) 237-247. https://doi.org/10.1016/j.msec.2014.11.024.
[12] A.K. Gain, L.C. Zhang, W.D. Liu, Microstructure and material properties of porous hydroxyapatite-zirconia nanocomposites using polymethyl methacrylate powders, Mater Design, 67 (2015) 136-144. https://doi.org/10.1016/j.matdes.2014.11.028.
[13] L. Chen, C. Deng, J. Li, Q. Yao, J. Chang, L. Wang, C. Wu, 3D printing of a lithium-calcium-silicate crystal bioscaffold with dual bioactivities for osteochondral interface reconstruction, Biomaterials, 196 (2019) 138-150. https://doi.org/10.1016/j.biomaterials.2018.04.005.
[14] P. Stastny, R. Sedlacek, T. Suchy, V. Lukasova, M. Rampichova, M. Trunec, Structure degradation and strength changes of sintered calcium phosphate bone scaffolds with different phase structures during simulated biodegradation in vitro, Mater Sci Eng C Mater Biol Appl, 100 (2019) 544-553. https://doi.org/10.1016/j.msec.2019.03.027.
[15] C. Piconi, G. Maccauro, Zirconia as a ceramic biomaterial, Biomaterials, 20 (1999) 1-25. https://doi.org/10.1016/S0142-9612(98)00010-6.
[16] J. Brzezinska-Miecznik, K. Haberko, M. Sitarz, M.M. Bucko, B. Macherzynska, R. Lach, Natural and synthetic hydroxyapatite/zirconia composites: A comparative study, Ceramics International, 42 (2016) 11126-11135. https://doi.org/10.1016/j.ceramint.2016.04.019.
[17] Y.M. Kong, C.J. Bae, S.H. Lee, H.W. Kim, H.E. Kim, Improvement in biocompatibility of ZrO2-Al2O3 nano-composite by addition of HA, Biomaterials, 26 (2005) 509-517. https://doi.org/10.1016/j.biomaterials.2004.02.061.
[18] V.A. Kumar, P.R.M. Raju, N. Ramanaiah, R. Siriyala, Effect of ZrO2 content on the mechanical properties and microstructure of HAp/ZrO2 nanocomposites, Ceramics International, 44 (2018) 10345-10351. https://doi.org/10.1016/j.ceramint.2018.03.045.
[19] S. Bose, M. Roy, A. Bandyopadhyay, Recent advances in bone tissue engineering scaffolds, Trends Biotechnol, 30 (2012) 546-554. https://doi.org/10.1016/j.tibtech.2012.07.005.
[20] A.C. Jones, C.H. Arns, D.W. Hutmacher, B.K. Milthorpe, A.P. Sheppard, M.A. Knackstedt, The correlation of pore morphology, interconnectivity and physical properties of 3D ceramic scaffolds with bone ingrowth, Biomaterials, 30 (2009) 1440-1451. https://doi.org/10.1016/j.biomaterials.2008.10.056.
[21] S. Lohfeld, S. Cahill, V. Barron, P. McHugh, L. Durselen, L. Kreja, C. Bausewein, A. Ignatius, Fabrication, mechanical and in vivo performance of polycaprolactone/tricalcium phosphate composite scaffolds, Acta Biomater, 8 (2012) 3446-3456. https://doi.org/10.1016/j.actbio.2012.05.018.
[22] R. Wang, P.F. Zhu, W.Y. Yang, S. Gao, B. Li, Q. Li, Direct-writing of 3D periodic TiO2 bio-ceramic scaffolds with a sol-gel ink for in vitro cell growth, Mater Design, 144 (2018) 304-309. https://doi.org/10.1016/j.matdes.2018.02.040.
[23] Z.B. Liu, H.X. Liang, T.S. Shi, D.Q. Xie, R.Y. Chen, X. Han, L.D. Shen, C.J. Wang, Z.J. Tian, Additive manufacturing of hydroxyapatite bone scaffolds via digital light processing and in vitro compatibility, Ceramics International, 45 (2019) 11079-11086. https://doi.org/10.1016/j.ceramint.2019.02.195.
[24] K.H. Hu, Y.M. Wei, Z.G. Lu, L. Wan, P.J. Li, Design of a Shaping System for Stereolithography with High Solid Loading Ceramic Suspensions, 3d Print Addit Manuf, 5 (2018) 311-318. https://doi.org/10.1089/3dp.2017.0065.

[25] E. Johansson, O. Lidstrom, J. Johansson, O. Lyckfeldt, E. Adolfsson, Influence of Resin Composition on the Defect Formation in Alumina Manufactured by Stereolithography, Materials (Basel), 10 (2017). https://doi.org/10.3390/ma10020138.

[26] W. Zhu, X. Ma, M. Gou, D. Mei, K. Zhang, S. Chen, 3D printing of functional biomaterials for tissue engineering, Curr Opin Biotechnol, 40 (2016) 103-112. https://doi.org/10.1016/j.copbio.2016.03.014.

[27] E.A. Olevsky, R.M. German, A. Upadhyaya, Effect of gravity on dimensional change during sintering—II. Shape distortion, Acta Materialia, 48 (2000) 1167-1180. https://doi.org/10.1016/S1359-6454(99)00369-9.

[28] E. Adolfsson, P. Alberius-Henning, L. Hermansson, Phase Analysis and Thermal Stability of Hot Isostatically Pressed Zirconia–Hydroxyapatite Composites, J Am Ceram Soc, 83 (2000) 2798 - 2802. https://doi.org/10.1111/j.1151-2916.2000.tb01634.x

[29] R.R. Rao, T.S. Kannan, Synthesis and sintering of hydroxyapatite–zirconia composites, Materials Science and Engineering C, 20 (2002) 187-193. https://doi.org/10.1016/S0928-4931(02)00031-0.

[30] S.-C. Wu, H.-C. Hsu, S.-K. Hsu, W.-H. Wang, W.-F. Ho, Preparation and characterization of four different compositions of calcium phosphate scaffolds for bone tissue engineering, Materials Characterization, 62 (2011) 526-534. https://doi.org/10.1016/j.matchar.2011.03.014.

[31] M. Inuzuka, Hydroxyapatite-doped zirconia for preparation of biomedical composites ceramics, Solid State Ionics, 172 (2004) 509-513. https://doi.org/10.1016/j.ssi.2004.01.054.

[32] J. Brzezinska-Miecznik, B. Macherzynska, R. Lach, B. Nowak, The effect of calcination and zirconia addition on HAp hot pressed materials, Ceramics International, 40 (2014) 15815-15819. https://doi.org/10.1016/j.ceramint.2014.07.108.

[33] D.J. Curran, T.J. Fleming, M.R. Towler, S. Hampshire, Mechanical properties of hydroxyapatite-zirconia compacts sintered by two different sintering methods, J Mater Sci Mater Med, 21 (2010) 1109-1120. https://doi.org/10.1007/s10856-009-3974-z.

[34] K. Castkova, H. Hadraba, A. Matousek, P. Roupcova, Z. Chlup, L. Novotna, J. Cihlar, Synthesis of Ca,Y-zirconia/hydroxyapatite nanoparticles and composites, Journal of the European Ceramic Society, 36 (2016) 2903-2912. https://doi.org/10.1016/j.jeurceramsoc.2015.12.045.

[35] S. Samavedi, A.R. Whittington, A.S. Goldstein, Calcium phosphate ceramics in bone tissue engineering: a review of properties and their influence on cell behavior, Acta Biomater, 9 (2013) 8037-8045. https://doi.org/10.1016/j.actbio.2013.06.014.

[36] K. Lin, C. Wu, J. Chang, Advances in synthesis of calcium phosphate crystals with controlled size and shape, Acta Biomater, 10 (2014) 4071-4102. https://doi.org/10.1016/j.actbio.2014.06.017.

[37] S.M. Best, A.E. Porter, E.S. Thian, J. Huang, Bioceramics: Past, present and for the future, Journal of the European Ceramic Society, 28 (2008) 1319-1327. https://doi.org/10.1016/j.jeurceramsoc.2007.12.001.

[38] M. Vallet-Regi, E. Ruiz-Hernandez, Bioceramics: from bone regeneration to cancer nanomedicine, Adv Mater, 23 (2011) 5177-5218. https://doi.org/10.1002/adma.201101586.

[39] C. Bao, X. Zhang, Research development and prospect of calcium phosphate biomaterials with intrinsic osteoinductivity, Sheng Wu Yi Xue Gong Cheng Xue Za Zhi, 23 (2006) 442-445, 454. https://doi.org/10.3321/j.issn:1001-5515.2006.02.049.

[40] S.H. Oh, I.K. Park, J.M. Kim, J.H. Lee, In vitro and in vivo characteristics of PCL scaffolds with pore size gradient fabricated by a centrifugation method, Biomaterials, 28 (2007) 1664-1671. https://doi.org/10.1016/j.biomaterials.2006.11.024.

[41] R. Taktak, A. Elghazel, J. Bouaziz, S. Charfi, H. Keskes, Tricalcium phosphate-Fluorapatite as bone

tissue engineering: Evaluation of bioactivity and biocompatibility, Mater Sci Eng C Mater Biol Appl, 86 (2018) 121-128. https://doi.org/10.1016/j.msec.2017.11.011.

[42] S.H. An, T. Matsumoto, H. Miyajima, A. Nakahira, K.H. Kim, S. Imazato, Porous zirconia/hydroxyapatite scaffolds for bone reconstruction, Dent Mater, 28 (2012) 1221-1231. https://doi.org/10.1016/j.dental.2012.09.001.

[43] T.J. Matsumoto, S.H. An, T. Ishimoto, T. Nakano, T. Matsumoto, S. Imazato, Zirconia-hydroxyapatite composite material with micro porous structure, Dent Mater, 27 (2011) e205-212. https://doi.org/10.1016/j.dental.2011.07.009.

[44] Z. Xia, L. Riester, W.A. Curtin, H. Li, B.W. Sheldon, J. Liang, B. Chang, J.M. Xu, Direct observation of toughening mechanisms in carbon nanotube ceramic matrix composites, Acta Materialia, 52 (2004) 931-944. https://doi.org/10.1016/j.actamat.2003.10.050.

[45] S. Qian, F. Liu, M. Ma, G. Chen, Z. Liu, Y. Li, Mechanical strength enhancement of low temperature co-fired multilayer ceramic substrates by introducing residual stress, Ceramics International, 45 (2019) 10982-10990. https://doi.org/10.1016/j.ceramint.2019.02.181.

[46] H.W. Kim, Y.J. Noh, Y.H. Koh, H.E. Kim, H.M. Kim, Effect of CaF on densification and properties of hydroxyapatite–zirconia composites for biomedical applications, Biomaterials, 23 (2002) 4113-4121. https://doi.org/10.1016/s0142-9612(02)00150-3

Figure Captions

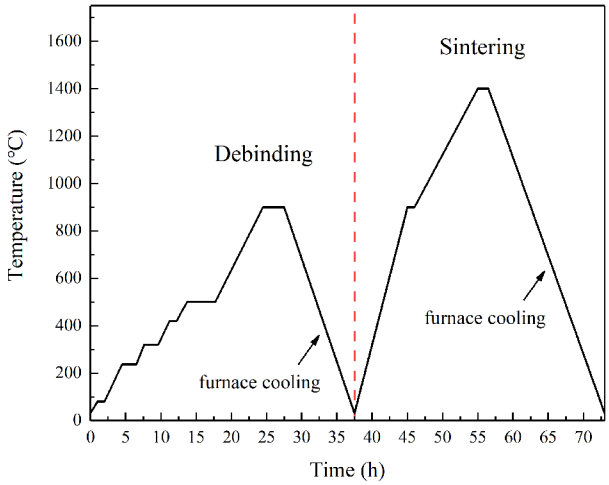

Fig. 1. Heating curve of debinding and sintering

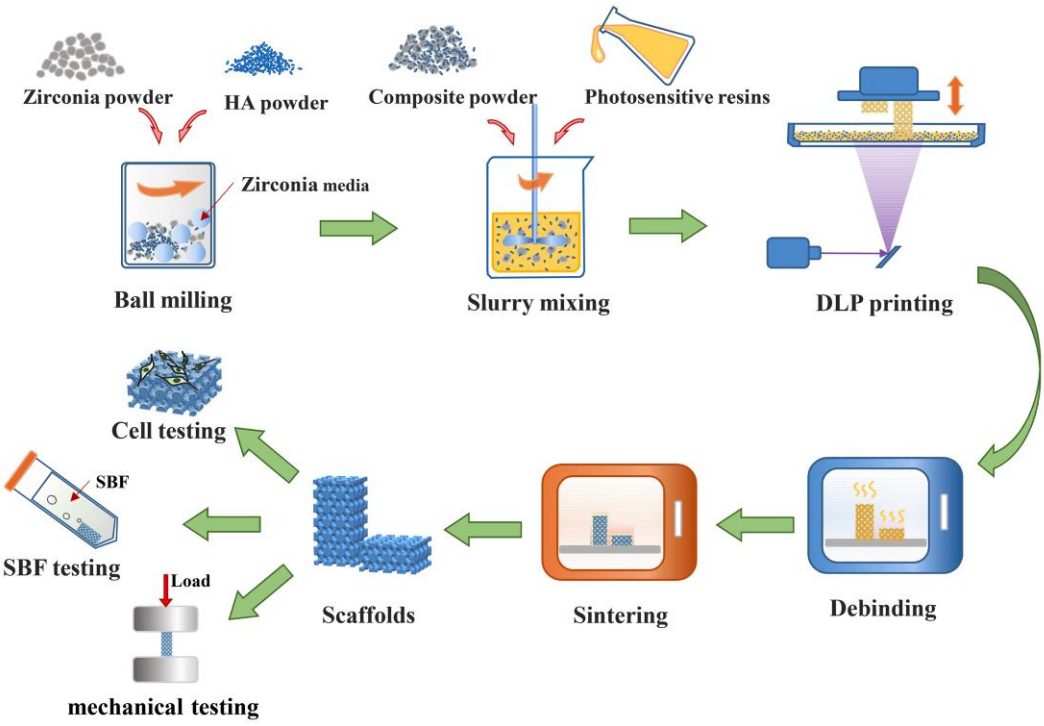

Fig. 2. Illustration of the fabrication and testing process.

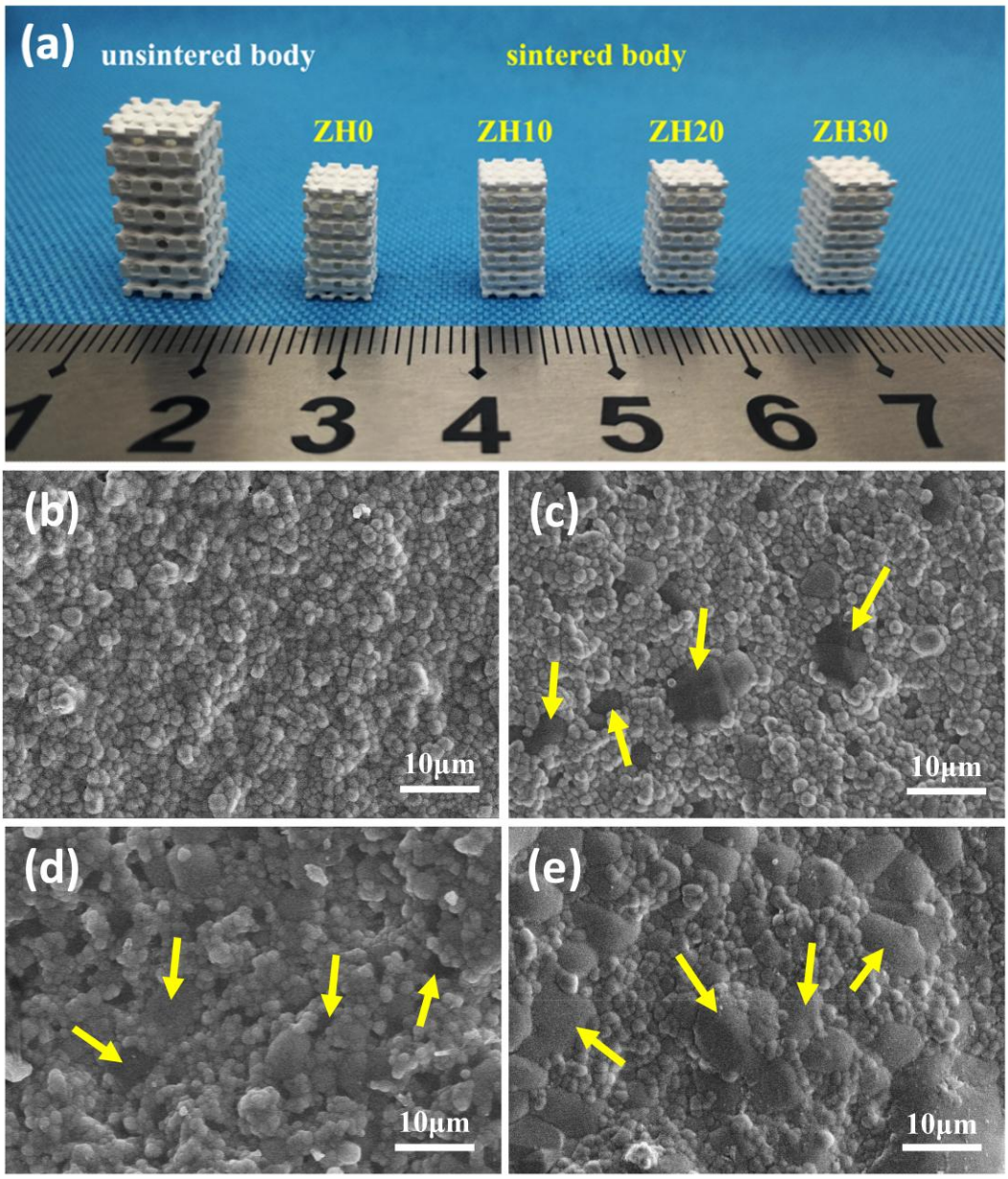

Fig. 3. Macroscopic and microscopic morphologies of the scaffolds:(a) Photos of scaffolds before and after sintering. SEM micrographs of (b) ZH0, (c) ZH10, (d) ZH20 and (e) ZH30 scaffolds. Arrows in the figure referred to the dark grains of different sizes embedded in the zirconia grains.

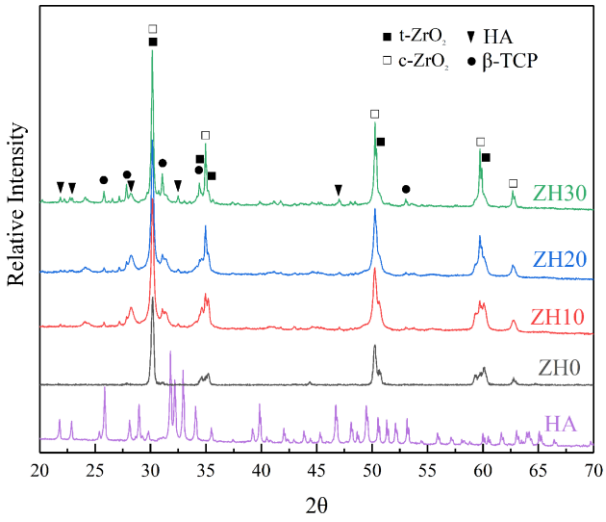

Fig. 4. XRD pattern of composite scaffolds after sintering

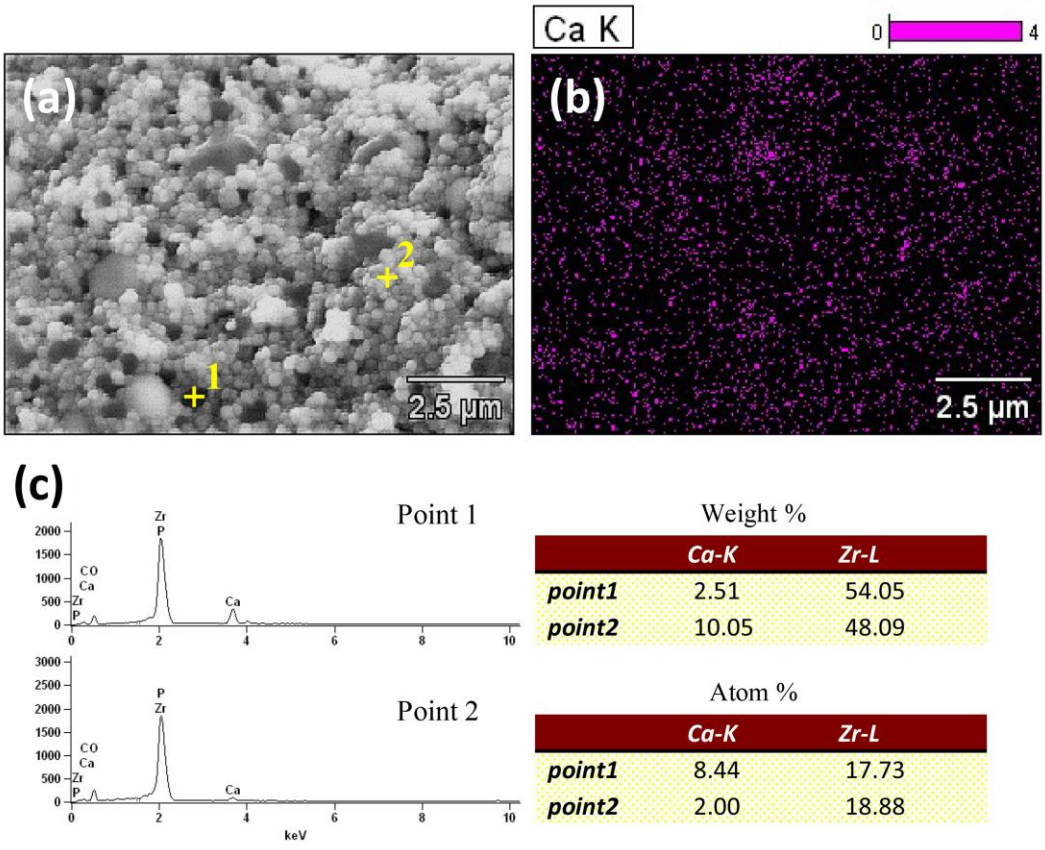

Weight %

	Ca-K	Zr-L
point1	2.51	54.05
point2	10.05	48.09

Atom %

	Ca-K	Zr-L
point1	8.44	17.73
point2	2.00	18.88

Fig. 5. EDS analyses of the elemental composition of the ZH20 scaffolds: (a) The surface area of the scaffold for elemental analysis. (b) Mapping image of calcium. (c) Elemental composition and content of

the designated areas (points 1 and 2) in figure (a).

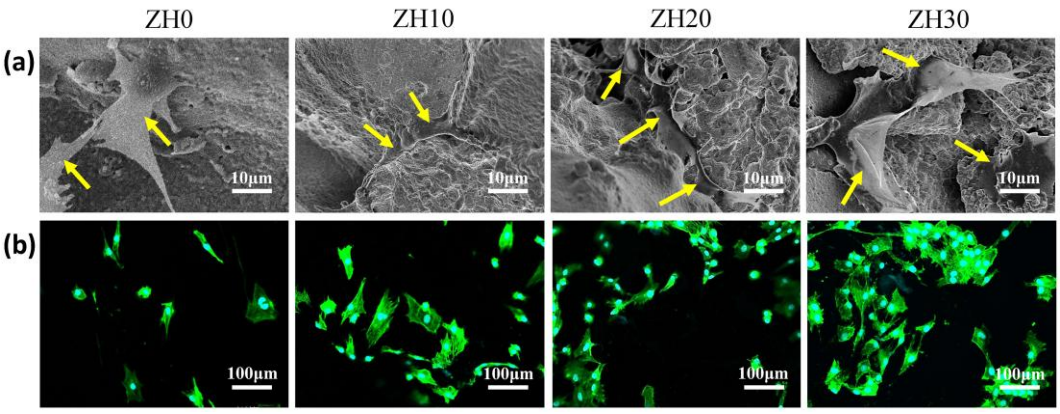

Fig. 6. (a) SEM images of cells pointed by arrows attached on the external surfaces of scaffolds after incubating for 1 day and (b) laser confocal images of cells attached on the internal surfaces of scaffolds after incubating for 4 days.

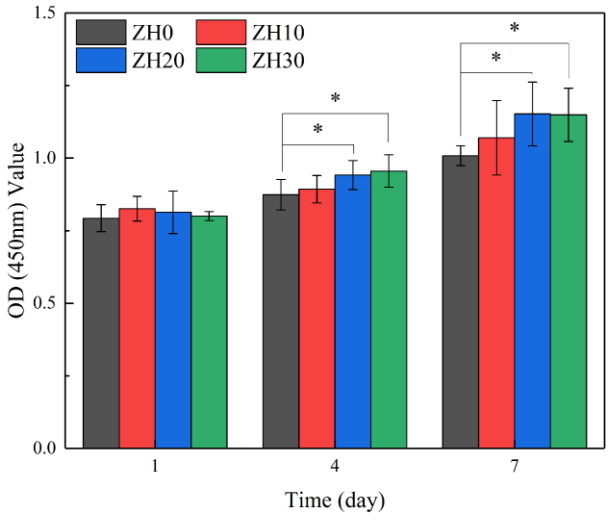

Fig. 7. Proliferation rate of MC3T3-E1 cells on scaffolds with different HA additions The values are represented as mean ± SD. (n = 5, * $p<0.05$).

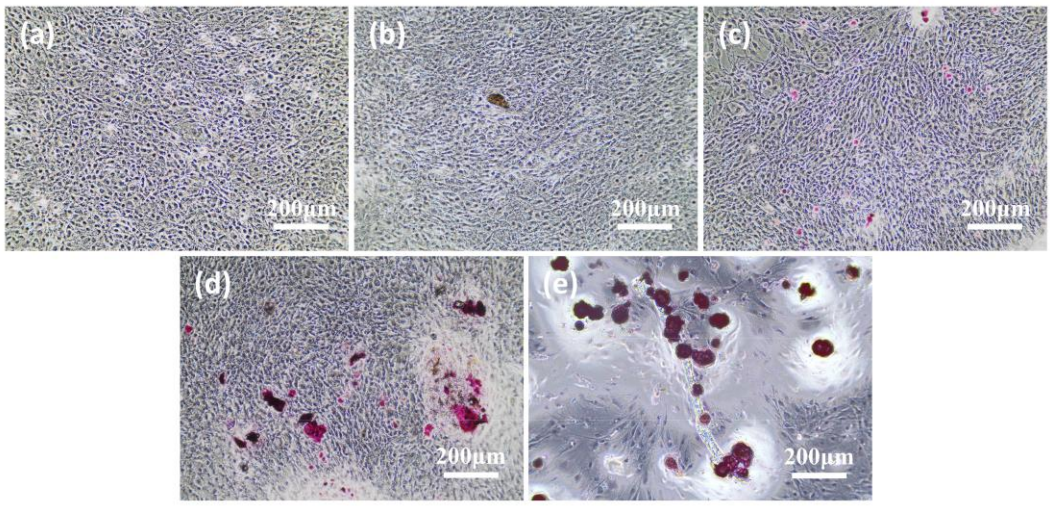

Fig. 8. The ARS staining images of MC3T3-E1 cells after incubation with (a) no scaffold, (b)ZH0, (c) ZH10, (d) ZH20 and (e) ZH30.

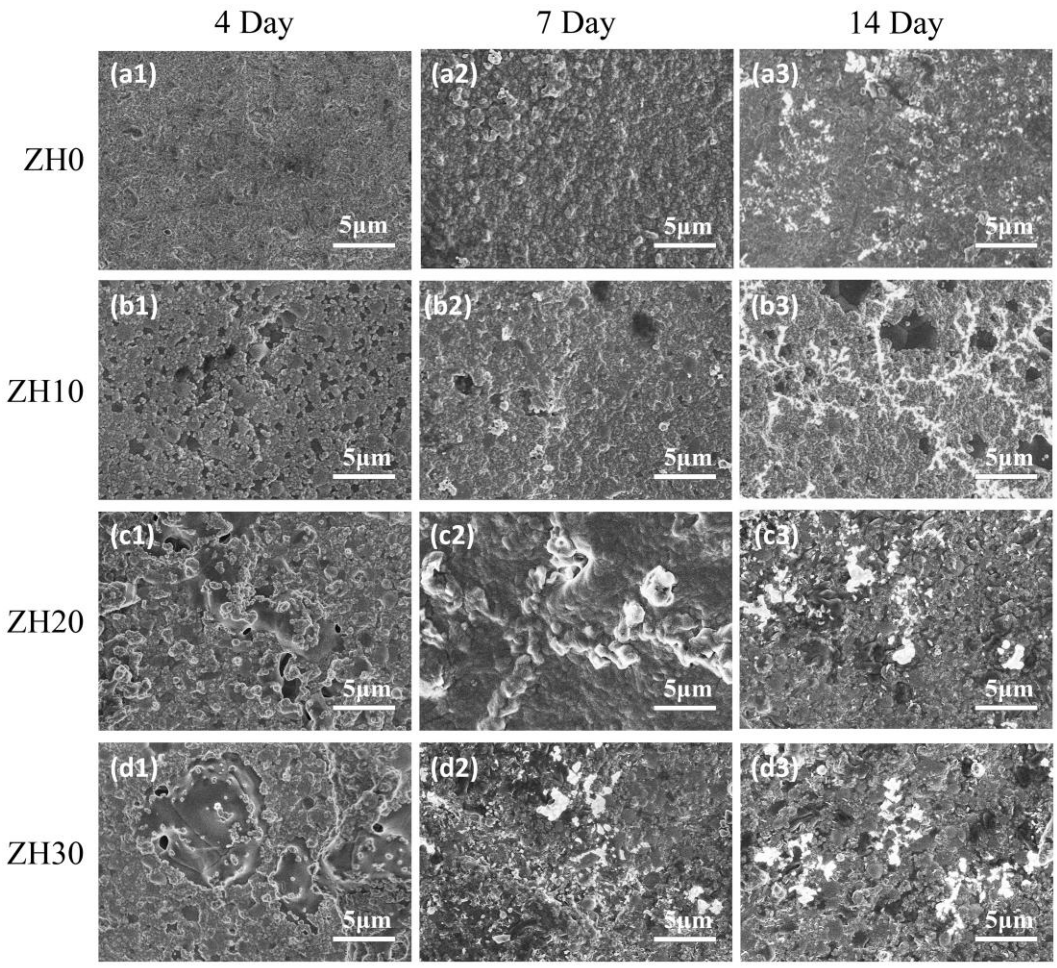

Fig. 9. SEM micrographs of the (a1-a3) ZH0, (b1-b3) ZH10, (c1-c3): ZH20 and (d1-d3) ZH30 scaffolds after soaking in SBF for 4, 7 and 14 days.

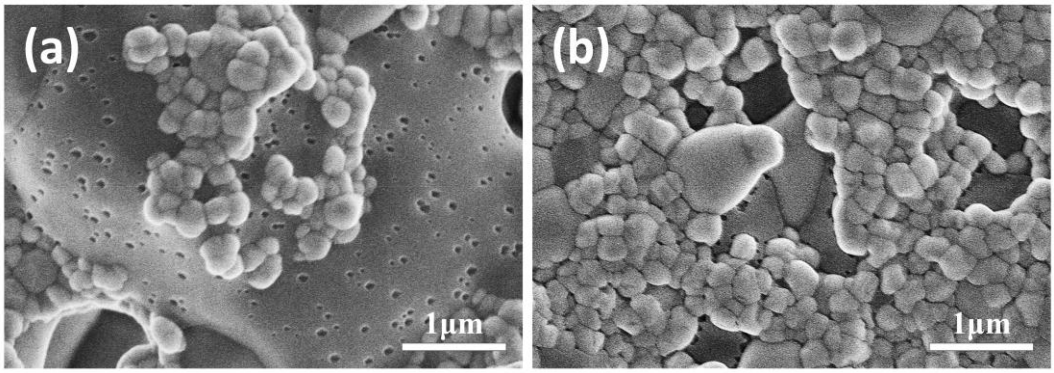

Fig. 10. SEM micrographs of calcium phosphate grains degradation: nano-scale micropores (a) on the surfaces and (b) at the boundaries of calcium phosphate grains.

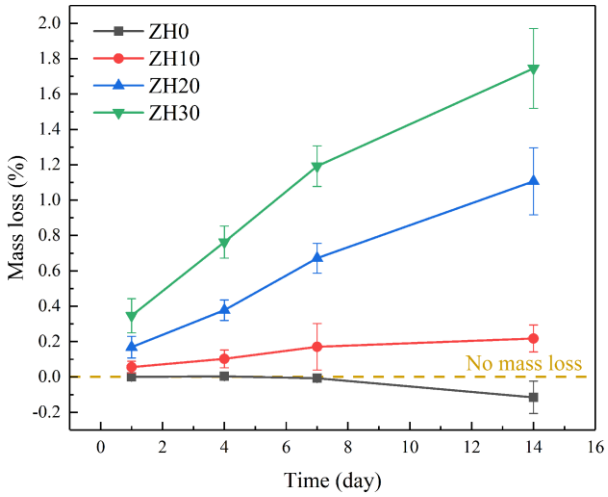

Fig. 11. The mass loss of scaffolds soaking in SBF for different time periods (n = 3).

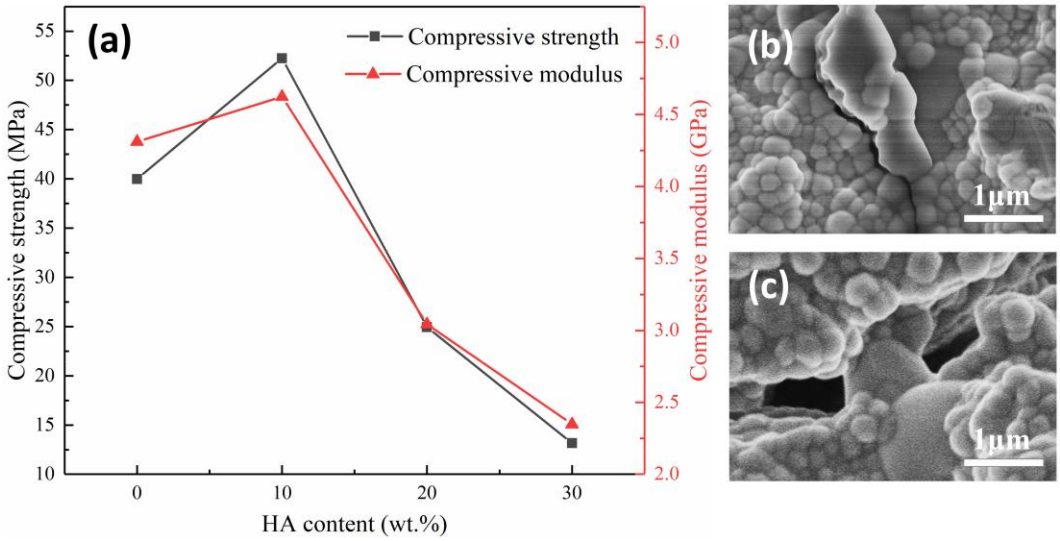

Fig. 12. (a) Compressive strength and compressive modulus of scaffolds as a function of HA content; SEM image of (b) crack deflection and (c) bridge on the ZH10 scaffold.

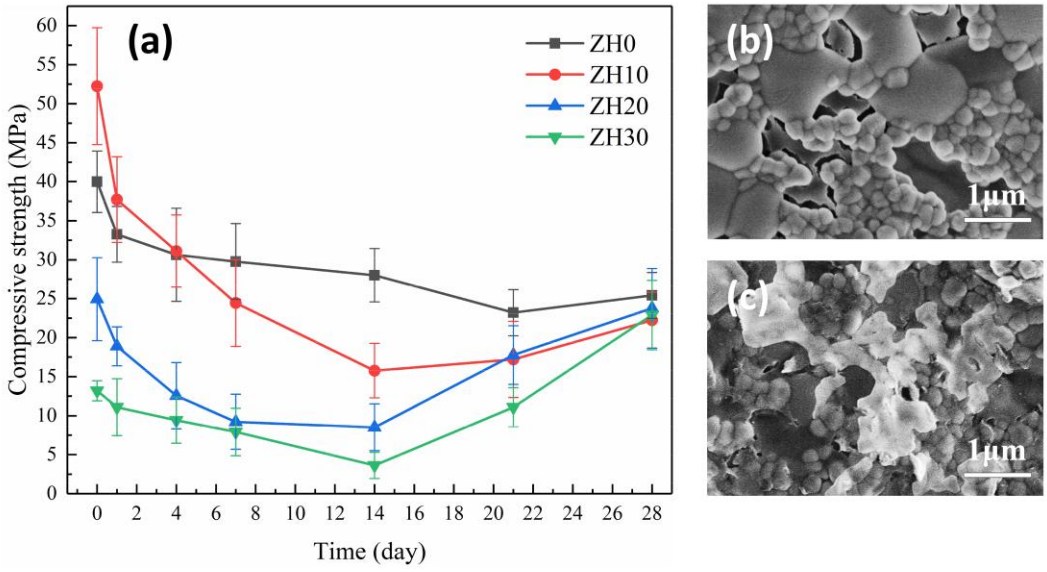

Fig. 13. (a) Compressive strengths of the scaffolds soaking in SBF for different time periods (n = 3). SEM micrographs of (b) degradation gaps and (c) apatite depositions filling the gaps.

Tables

Table 1. Dimensions of the model, unsintered and sintered bodies

	Model	Unsintered body	Sintered body	Shrinkage(%)
Length (mm)	7.5	7.35	5.64	23.27
Height (mm)	15	15	10.75	28.33